Xiong, C., Stolle, C., Lühr, H. (2016): The Swarm satellite loss of GPS signal and its relation to ionospheric plasma irregularities. - *Space Weather*, *14*, 8, pp. 563—577.

DOI: http://doi.org/10.1002/2016SW001439

AGU PUBLICATIONS

Space Weather

RESEARCH ARTICLE
10.1002/2016SW001439

Key Points:
- The total loss of GPS signal is frequently observed by the receivers on board Swarm satellites
- The total loss of GPS signal events at low latitudes are all related to equatorial plasma irregularities
- The total loss of GPS signal events at high latitudes are possibly related to polar patches and magnetic disturbances

Correspondence to:
C. Xiong,
bear@gfz-potsdam.de

Citation:
Xiong, C., C. Stolle, and H. Lühr (2016), The *Swarm* satellite loss of GPS signal and its relation to ionospheric plasma irregularities, *Space Weather*, *14*, 563–577, doi:10.1002/2016SW001439.

Received 2 JUN 2016
Accepted 26 JUL 2016
Accepted article online 1 AUG 2016
Published online 13 AUG 2016

The *Swarm* satellite loss of GPS signal and its relation to ionospheric plasma irregularities

Chao Xiong[1], Claudia Stolle[1,2], and Hermann Lühr[1]

[1]GFZ German Research Centre for Geosciences, Potsdam, Germany, [2]Faculty of Science, University of Potsdam, Potsdam, Germany

Abstract In this study we investigated conditions for loss of GPS signals observed by the *Swarm* satellites during a 2 year period, from December 2013 to November 2015. Our result shows that the *Swarm* satellites encountered most of the total loss of GPS signal at the ionization anomaly crests, between ±5° and ±20° magnetic latitude, forming two bands along the magnetic equator, and these low-latitude events mainly appear around postsunset hours from 19:00 to 22:00 local time. By further checking the in situ electron density measurements of *Swarm*, we found that practically, all the total loss of GPS signal events at low latitudes are related to equatorial plasma irregularities (EPIs) that show absolute density depletions larger than 10×10^{11} m^{-3}; then, the *Swarm* satellites encountered for up to 95% loss of GPS signal for at least one channel and up to 45% tracked less than four GPS satellites (making precise orbit determination impossible). For those EPIs with density depletions less than 10×10^{11} m^{-3}, the chance of tracked GPS signals less than four reduces to only 1.0%. *Swarm* also observed total loss of all GPS signal at high latitudes, mainly around local noon, and these events are related to large spatial density gradients due to polar patches or increased geomagnetic/auroral activities. We further found that the loss of GPS signals were less frequent after appropriate settings of the *Swarm* GPS receivers had been updated. However, the more recent period of the mission, e.g., after the GPS receiver settings have been updated, also coincides with less severe electron density depletions due to the declining solar cycle, making GPS loss events less likely. We conclude that both lower electron density gradients and appropriate GPS receiver settings reduce the probability for Swarm satellites loss of GPS signals.

1. Introduction

Ionospheric scintillations are one of the earliest known effects of space weather. Earlier studies related to scintillation effects on communication signals were mainly for very high frequency and ultrahigh frequency radio bands [e.g., *Whitney and Basu*, 1977; *Aarons*, 1982]. However, during the last few decades with the development of Global Navigation Satellite Systems (GNSS), scintillations on L band have also been frequently observed from both ground-based and spaceborne receivers [e.g., *Basu et al*., 1980; *Aarons and Basu*, 1994; *Kintner et al*., 2004; *Dymond*, 2012]. From a global view, scintillations on GNSS systems are more severe and frequent at low latitudes, particularly during postsunset hours and high solar activity years [*Basu et al*., 2002]. At high latitudes scintillations occur but less severe in magnitude [*Kintner et al*., 2007; *SBAS Ionospheric Working Group*, 2010]. Scintillations on GNSS systems are rarely experienced at middle latitudes, but have also been reported during intense magnetic storm periods, e.g., due to traveling ionospheric disturbances caused by high-latitude ionospheric structures [*Jakowski et al*., 2012; *Pradipta et al*., 2016].

Scintillation effects can be broadly classified as refraction and diffraction, and both types are originating from the group delay and phase advance as the GNSS signal is interacting with free electrons along its transmission path [*Kintner et al*., 2007]. At low latitudes, scintillations on GNSS systems are usually considered to be caused by ionospheric weather phenomena such as sporadic *E* (E_s), equatorial plasma irregularities (EPIs), or the equatorial ionization anomaly (EIA) [e.g., *Yue et al*., 2016]. When the GNSS radio wave traverses the ionospheric plasma irregularities, the phase along the wavefront varies. As the waves continue propagating through the ionosphere, they emerge from different points along the transmission path due to the refraction of the wave path. This effect, producing fluctuations of the signal amplitude, can degrade signal quality or causes failure of signal tracking. This process is often called "loss of lock," which may increase the navigation errors or, in some cases, cause navigation failure. Therefore, acquiring or reacquiring GNSS satellite signals becomes a severe space weather phenomenon.

EPIs are mainly generated from the bottomside of the ionospheric *F* region at the magnetic equator after sunset hours and later extend to higher altitudes [e.g., *Kelley*, 2009]. Their climatology has widely been studied previously. At low Earth orbit (LEO) satellite altitudes, the occurrence rate of EPIs increases rapidly around 19:00 LT (local time) and the highest rate is usually observed around 21:00 LT; afterward it decays slowly and lasts to postmidnight hours [e.g., *Kil and Heelis*, 1998; *Burke et al*., 2004; *Stolle et al*., 2006]. The occurrence of EPIs shows typical seasonal/longitudinal distributions. During June (December) solstice the EPI occurrence rate reaches highest values in the African and Pacific (South America and Atlantic) regions, while during equinoxes the occurrence rate is generally higher than that during solstices but with smaller longitude dependence [*Huang et al*., 2001; *Burke et al*., 2004; *Su et al*., 2006; *Stolle et al*., 2008; *Xiong et al*., 2010]. Studies focusing on the relation between EPIs and GNSS signal scintillations have also been published. The climatology of ionospheric scintillations at spaceborne GPS receivers was presented by *Dymond* [2012] and *Carter et al*. [2013]. With the amplitude scintillation index, S_4, derived from the Constellation Observing System for Meteorology, Ionosphere, and Climate (COSMIC) satellites, *Brahmanandam et al*. [2012] found that the maximum S_4 index appeared near the magnetic equator in the altitude range of 200–400 km. *Huang et al*. [2014] reported that the S_4 index derived from COSMIC showed similar local time variations as the occurrence of EPIs observed by the Communications/Navigation Outage Forecasting System satellite.

Buchert et al. [2015] reported that the recently launched *Swarm* satellites repeatedly encountered loss-track of GPS signals during January and February 2014. From an event study they showed that these loss-track of GPS signals occurred right at plasma density gradients associated with ionospheric plasma irregularities. After more than 2 years in space, GPS loss-track events were observed regularly by *Swarm*, allowing us to investigate their global distributions, as well as the seasonal and local time dependencies. In this study we are not focusing on the transient loss of GPS tracking loop or cycle slip (the discontinuity for a measured carrier phase) that has been published earlier [e.g., *Yue et al*., 2016]. This paper will explicitly focus on the total loss of signal from all GPS satellites (data gap) and the reduction to less than four satellites that makes the precise orbit determination (POD) for *Swarm* impossible. In parallel to these events, we investigate the *Swarm* in situ electron density measurements and provide quantitative information of electron density gradient associated with EPIs causing the *Swarm* satellites loss of GPS signal.

In the sections to follow we first introduce the data set and the approach for finding the loss of GPS signal events. The comparisons between these events and ionospheric plasma irregularities as well as the relevant discussions are given in section 3. Finally, we summarize the main findings from our results in section 4.

2. Data Set and Processing Approach

2.1. *Swarm* Satellite Mission and Onboard GPS Receivers

The *Swarm* mission, comprising three spacecraft, was launched on 22 November 2013 into a near-polar (87.5° inclination) orbit with initial altitude of about 500 km. From January 2014 onward the three spacecraft were maneuvered apart and achieved their final constellation on 17 April 2014. From then on the lower pair, *Swarm* A and C, was flying side by side at an altitude of about 470 km, with longitudinal separation of about 1.4° (about 150 km). The third spacecraft, *Swarm* B, orbits the Earth at about 520 km with a higher inclination. For covering all 24 h local times, *Swarm* A and C need about 133 days and *Swarm* B needs about 141 days. The in situ plasma density is measured by the two Langmuir probes of the Electric Field Instrument, with a time resolution of 2 Hz.

All three *Swarm* satellites carry dual-frequency GPS receivers of the same type including an antenna on the topside looking upward into the ionosphere and plasmasphere. The GPS receivers are equipped with eight channels, which means that the *Swarm* satellites can simultaneously receive signal from at most eight GPS satellites. Before *Swarm* was launched into space, GPS satellite simulator tests based on realistic scenarios were applied to the receivers during ground test campaign, including space-environmental testing (thermal vacuum and vibration). The behavior of the receivers on board *Swarm* A, B, and C appeared to be highly comparable [*Sust et al*., 2014; *Buchert et al*., 2015].

During the earlier mission phase all three *Swarm* satellites delivered GPS data with a time resolution of 10 s; later on 15 July 2014 the receiver configuration was changed, and since then all *Swarm* satellites are delivering 1 s GPS data [*Van den Ijssel et al*., 2015]. The initial field of view (FOV) of *Swarm* GPS receivers was limited to

80°. Now it has been updated several times during the past 2 years, and finally, the FOV of *Swarm* C has been increased to 88° on 13 January 2015 and on 6 May 2015 for *Swarm* A and B. Also, the phase-locked loop (PLL) bandwidth of *Swarm* C has been updated on 6 May 2015, with L1 PLL bandwidth increased from 10 Hz to 15 Hz and L2 PLL bandwidth increased from 0.25 Hz to 0.5 Hz. The details of the *Swarm* GPS receiver updates can be found in *Van den Ijssel et al*. [2016]. Before this update a restart of the receiver occurred when less than three GPS signals were received at the same time. Now after losing track to a GPS satellite the *Swarm* receiver will try 3 times to reacquire the signal again and only restarts when absolutely no GPS signal is recorded. Similar updates of the GPS receivers on board *Swarm* A and B have been carried out on 8 and 10 October 2015, respectively. Possible effects on the occurrence of loss of GPS signals through these adjustments are discussed in section 3.4.

2.2. Loss of GPS Signal Event Detection

For detecting the *Swarm* loss of GPS signal events we used the *Swarm* level 1b GPS observation data (receiver-independent exchange (RINEX) 3.00 file: GPSx_RO_1B). These files provide the GPS quantities: carrier phase of C/A code on L1 frequency (L1C), carrier phase of P code on L2 frequency (L2P), pseudo-range of C/A and P codes on L1 frequency (C1C and C1P), pseudo-range of P code on L2 frequency (C2P), signal strength of C/A and P codes on L1 frequency (S1C and S1P), and signal strength of P code on L2 frequency (S2P). Detailed description of RINEX 3.00 file can be found at ftp://ftp.unibe.ch/aiub/rinex/rinex300.pdf. A GPS satellite associated to a certain pseudo-range number (PRN) whose signals can potentially be received by the receiver is called to be "in the field of view," and the GPS satellite is called "visible satellite." Thus, for each epoch (every 10 s before 15 July 2014 and every 1 s thereafter), the *Swarm* RINEX files provide the number of visible GPS satellites and report the observations of the corresponding quantities on L1 and L2. Loss of signal is then identified by an interruption (missing epoch) of the received signal that lasts less than a certain period ($\Delta t_{max} = 30$ min); hence, the satellite becomes visible again within this time period. If two loss events occur close to each other (less than 60 s apart), they are combined and considered as one event. We identified various durations of loss of all signals from a few seconds to a couple of minutes. If lost signals from a GPS satellite are not retracked after 30 min, the GPS satellite is considered to have become out of the field of view of the *Swarm* GPS receiver.

Figure 1 presents the two examples of loss of GPS signal observed by *Swarm* A. The first event was observed on 30 October 2014. Here *Swarm* A was in the descending orbit around −78.8°E longitude, and the magnetic latitude (MLAT) covered by *Swarm* A was from 33° to −47°during the considered period (from 01:15 to 01:36 UTC). The signal strength (carrier-to-noise density ratio for P code of L1 frequency) and elevation angle of the visible GPS satellites are shown by the solid black and red lines, respectively. Intervals of loss of GPS signal for the different PRNs are indicated by dot-dashed lines. For example, the signal from PRN = 18 was interrupted around 01:27 UTC, the signal of PRN = 25 was interrupted twice around 01:21 and 01:27 UTC, and the signal of PRN 31 was interrupted around 01:21 UTC. Similarly, the GPS signal interruptions also occurred for PRN = 14, 21, and 29, with shorter durations. The signals of PRNs 12, 22, and 24 have been lost without being reacquired and are considered to be out of the field of view, and those examples are not identified as an intermediate loss of signal in the following analyses. In this example at least one GPS satellite has been received during the entire segment of *Swarm* orbit shown, and therefore, loss of all GPS signals did not occur. During the intervals of signal interruption, the elevations angles of GPS satellites are larger than 30°, implying that the GPS signal loss are not caused by the low-elevation angle, such as due to possible enhanced reflections on the satellite body. Ionospheric effects along the signal path from GPS satellites to *Swarm* receivers are more likely to cause the signal interruptions.

Figure 1b presents an example of loss of GPS signal observed on 27 October 2014. *Swarm* A was in the descending orbit around −21.5°E longitude, and the magnetic latitude (MLAT) covered by *Swarm* A was from 49° to −35°during the considered period (from 21:30 to 21:51 UTC). Signal interruptions were recorded for different GPS satellites, and some of the GPS signals interrupted several times during the considered period (e.g., PRN = 02, 05, 06, 10, 13, 15, 24, 26, 28, and 30). In this example, the signals from all visible GPS satellites were interrupted from 21:44:03 to 21:45:33 UTC (marked by the gray bar). Such time intervals are considered as total loss of GPS signals in the following analyses.

The examples presented above indicate that the GPS signals received by *Swarm* receivers can be interrupted at some or even all channels. Figure 1c presents the percentage of tracked GPS satellites during a 2 year

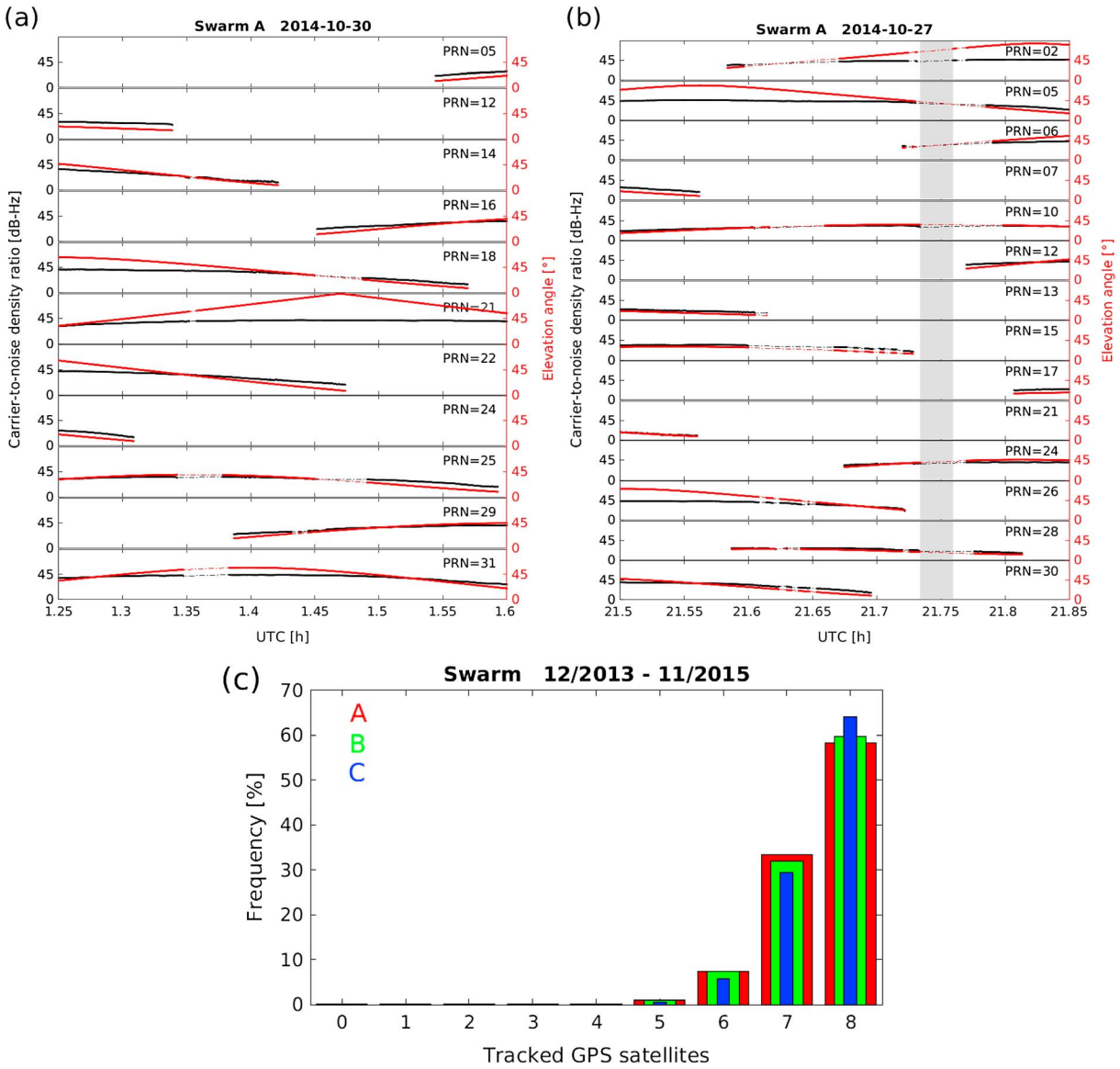

Figure 1. Two examples of GPS signal loss observed by *Swarm*. (a) Signal strength from some of the GPS satellites is interrupted (indicated by the dot-dashed intervals). (b) Signal from all visible GPS satellites are totally interrupted at the same time (indicated by the gray bar). The black and red curves represent the signal strength (carrier-to-noise density ratio) and elevation angle of each visible GPS satellite, respectively. (c) GPS tracking performance of *Swarm* receivers during a 2 year period, from December 2013 to November 2015.

period, from December 2013 to November 2015. The histogram indicates that for more than half of the time (58.3%, 59.8%, and 64.2% for the three satellites, respectively) the *Swarm* receivers can track eight GPS satellites. But there were also time (2.3%, 0.8%, and 2.6%) that *Swarm* tracked less than four GPS satellites when POD is impossible, and among them there were 65, 22, and 79 events found with total loss of GPS signal at all eight channels. In the next section we focus on these total loss of GPS signal events and investigate their global distributions, the seasonal and local time dependencies, and their relation to the ionospheric plasma irregularities.

3. Results and Discussion

3.1. The Characteristics of *Swarm* Satellite Loss of GPS Signal

Figure 2 presents the global distribution of GPS loss of signal events for all channels observed by the three *Swarm* satellites, where dots are located at the midpoint between start and end of the interruptions. The

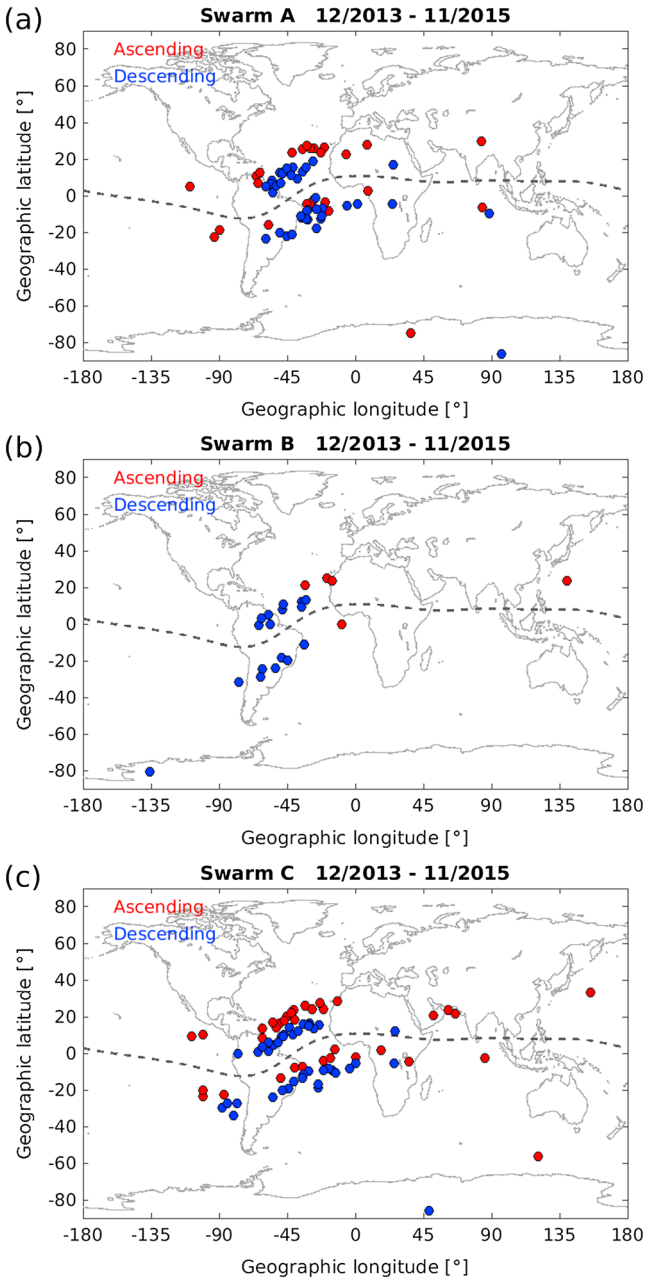

Figure 2. (a–c) The global distributions of GPS signal total interruption for all channels observed by *Swarm* satellites. For each *Swarm* satellite the events have been marked with blue and red dots for separating the ascending and descending orbital arcs, respectively. The gray dashed line in each panel represents the magnetic equator.

events are marked by blue and red colors for separating ascending (from south to north) and descending (from north to south) orbital arcs, respectively. Most of the events are observed at low latitudes between ±5° and ±20° MLAT, distributed as two bands north and south of the magnetic equator and are mainly grouped at longitudes between −90°E and 0°E (especially for *Swarm* B). The events from ascending nodes are located a few degrees further northward than the events from the descending nodes. As we will see later this shift can be explained by the satellite flying into an ionospheric irregularity and taking some time to reacquire signals. On average this occurs more toward north for events from ascending nodes. At high latitudes only five events are observed by the three *Swarm* satellites, and all of them occur in the southern hemisphere.

Figure 3 presents the MLAT versus magnetic local time (MLT) distribution of GPS signal total interruption events for the three *Swarm* satellites. The magnetic latitude and magnetic local time we used is based on the apex or quasi-dipole magnetic field coordinates, which have been defined by *Richmond* [1995] and updated by *Emmert et al.* [2010]. All events at low latitudes appear during postsunset hours, roughly from 18:30 to 22:00 MLT. The high-latitude events mainly appear around local noon and one event observed by *Swarm* C around midnight.

Figure 4 shows the seasonal and longitudinal distributions of these GPS signal total interruption events marked with different colors for the three *Swarm* satellites. As already recognized in Figure 2, they are mainly located at longitudes between −90°E and 0°E and concentrate on equinox with day of year from 30 to 100 and from 290 to 330. The considered period of 2 years is, however, too short for deriving a proper seasonal distribution.

The distributions of these GPS signal total interruption events at equatorial latitudes observed by the *Swarm* satellites are consistent with the distribution of the equatorial plasma irregularities detected on board LEO satellites, which have been reported by many previous studies [e.g., *Burke et al.*, 2004; *Stolle et al.*, 2006; *Su et al.*, 2006; *Xiong et al.*, 2010]. Already from this climatological view, there is a clear hint that equatorial plasma density irregularities and GPS loss of signal are close related. In the next subsection we will address the relation between the two phenomena in more detail.

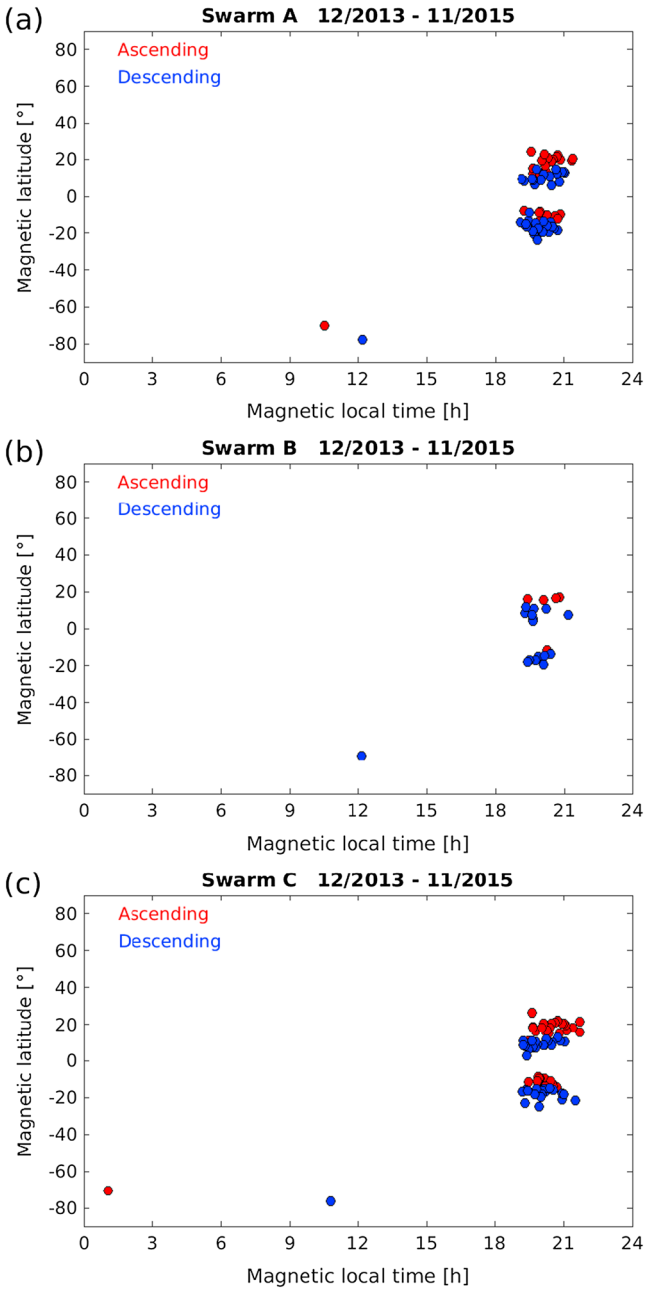

Figure 3. (a–c) The magnetic latitude versus magnetic local time distributions of the total loss of GPS signal events. The blue and red dots indicate the events for the ascending and descending orbital arcs, respectively.

3.2. The Loss of GPS Signal at Low Latitudes and Their Relation with Equatorial Plasma Irregularity

The GPS signals are affected by the plasma variations along the signal path. Therefore, the total electron content (TEC) is suitable for representing the variations along the signal path. However, when the GPS signal drops out, there is no information on the carrier and TEC cannot be derived. Instead, the Langmuir probes on board the *Swarm* satellites provide in situ plasma density measurements independently of GPS observations and enable us to monitor density variations before and throughout GPS outage. For satellites in the topside ionosphere the electron density in the vicinity of the spacecraft makes major contributions to the TEC results, as has been shown in *Noja et al.* [2013, Figure 8] for high latitudes. Similar relations are valid at low latitude. Figure 5 shows one example of comparison between in situ electron density (N_e) and slant TEC variations separately for *Swarm* A and C. Although the two spacecraft are separated by only 150 km in longitude, *Swarm* A passes through region with EPIs, while *Swarm* C does not. For both spacecraft, the TEC from PRN = 1 follow the in situ electron density variations and reproduce most of the details but with smoother amplitudes; however, markedly difference of TEC is found between *Swarm* A and C. This example demonstrates how much the TEC values are influenced by the electron density in close vicinity to the *Swarm* spacecraft. In the following, we will therefore compare the in situ electron density and its effect on GPS receivers.

For detecting EPIs from *Swarm* electron density data we used the same approach as introduce by *Xiong et al.* [2016]. The N_e time series from each equatorial orbital segment (within ±40° MLAT) are first high-pass filtered with a cutoff period of 40 s (corresponding to an along-track wavelength of about 300 km). Subsequently, the filtered signal is rectified. Values exceeding an upper limit (UL) are first identified as a possible EPI event. For each event, the rectified signal should have multipeaked values above UL, and this event is limited along the orbit by rectified signals below a lower limit (LL) for at least 3° north and south of the event. Otherwise, the fluctuations of rectified signal are attributed to enhanced noise and are considered as not significant. The thresholds of UL and LL are set here to $3\times10^{10}\,m^{-3}$ and $1.5\times10^{10}\,m^{-3}$, respectively, which are mainly estimated from the level of quiet time N_e variations at *Swarm* altitudes.

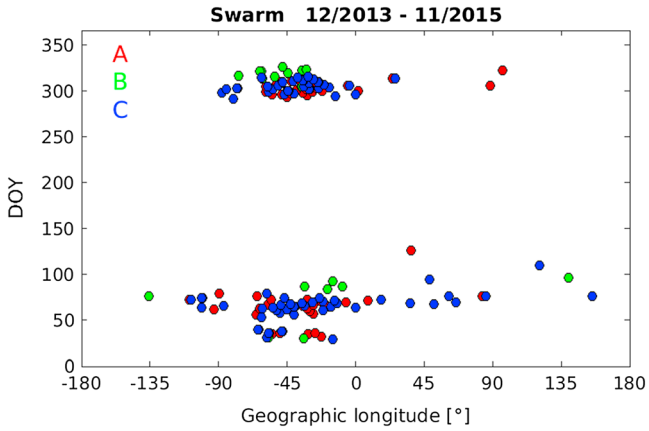

Figure 4. The seasonal versus longitudinal distribution of total loss of GPS signal events. The different colors indicate the events observed by the three different *Swarm* satellites.

With the approach described above, we found that EPIs are detected for all the total loss of GPS signal events. Correspondingly, the official *Swarm* level 2 product termed ionospheric bubble index [see *Park et al.*, 2013], providing routinely time and location of strong equatorial plasma irregularities detected in the magnetic field and electron density, identified "bubbles" for each of the total loss of GPS signal event.

3.2.1. Examples

Figure 6a presents an EPI example from both the electron density (black) and slant TEC from PRN = 31 (red) observations for *Swarm* A and C on 07 March 2015. Here the satellites have been in ascending orbit. The intervals with GPS signal total interruption are indicated by the gray bars, which happened from 22:44:26 to 22:47:41 UTC in the southern and from 22:53:27 to 22:54:57 UTC in the northern hemisphere for *Swarm* A and from 22:52:55 to 22:55:42 UTC in the northern hemisphere for *Swarm* C. At those locations clear in situ density depletions are found for both satellites: in the southern hemisphere along the *Swarm* A path between −17.6° and −10.4° MLAT and in the northern hemisphere between 11.6° and 17.7° MLAT for *Swarm* A and between 4.1° and 17.4° MLAT for *Swarm* C. The slant TEC for both spacecraft shows also clear variations, indicating the GPS ray has passed through regions of intense electron density gradient. Notable as well is that the observed density depletion structures are quite different in depths and spatial scales between the satellites. From a statistical analysis focusing on the scale size of EPIs observed by *Swarm* A and C, *Xiong et al.* [2016] showed that plasma irregularities are usually uncorrelated between the two satellites, although they are separated by only about 150 km in longitude.

Figures 6b and 6c show the carrier-to-noise density ratio of the P code on the L1 frequency (black lines) and the elevation angle (red lines) of each visible GPS satellite during the considered period, observed by *Swarm* A and C, respectively. Similar to Figure 1, the dot-dashed lines indicate the signal loss of the corresponding GPS satellites, and the gray bars indicate the intervals when the loss of GPS signal is observed at all channels.

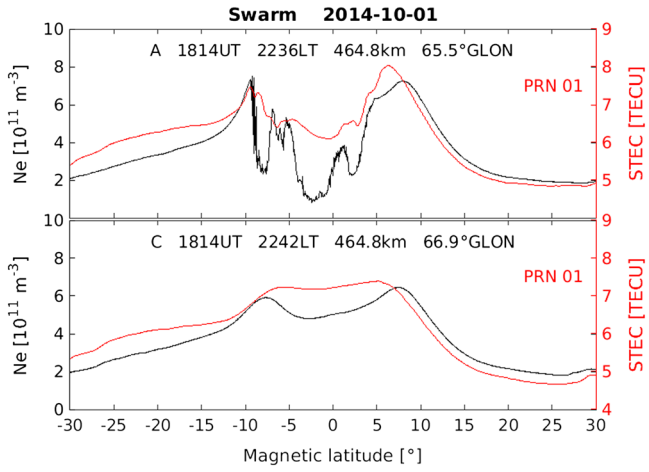

Figure 5. Comparison of in situ electron density measurements (black) with the slant TEC (red) profiles from *Swarm* (top) A and (bottom) C. The time and location on the top refer to the geographic equator crossing of the satellites. TEC profiles tracked the local plasma density variations quite well.

During the first indicated interval (around 22:45 UTC) on the southern hemisphere some of the GPS satellites are out the field of view for *Swarm* A (e.g., PRN = 01, 09, 16, 21, 23, and 32); therefore, their signal cannot be received. For other GPS satellites (e.g., PRN = 04, 11, 14, 19, 27, and 31), the signal is interrupted and reacquired again afterward; however, at the same time, the signal from PRN = 14 and 31 is still received by *Swarm* C. Compared to the distance from the GPS satellite to *Swarm* (about 21,500 km), the longitudinal separation between *Swarm* A and C (about 150 km) is small, and the signals from the same GPS satellite received by *Swarm* A and C can be considered to follow practically the same propagation path. As seen from Figure 6a, *Swarm* A observed clear density

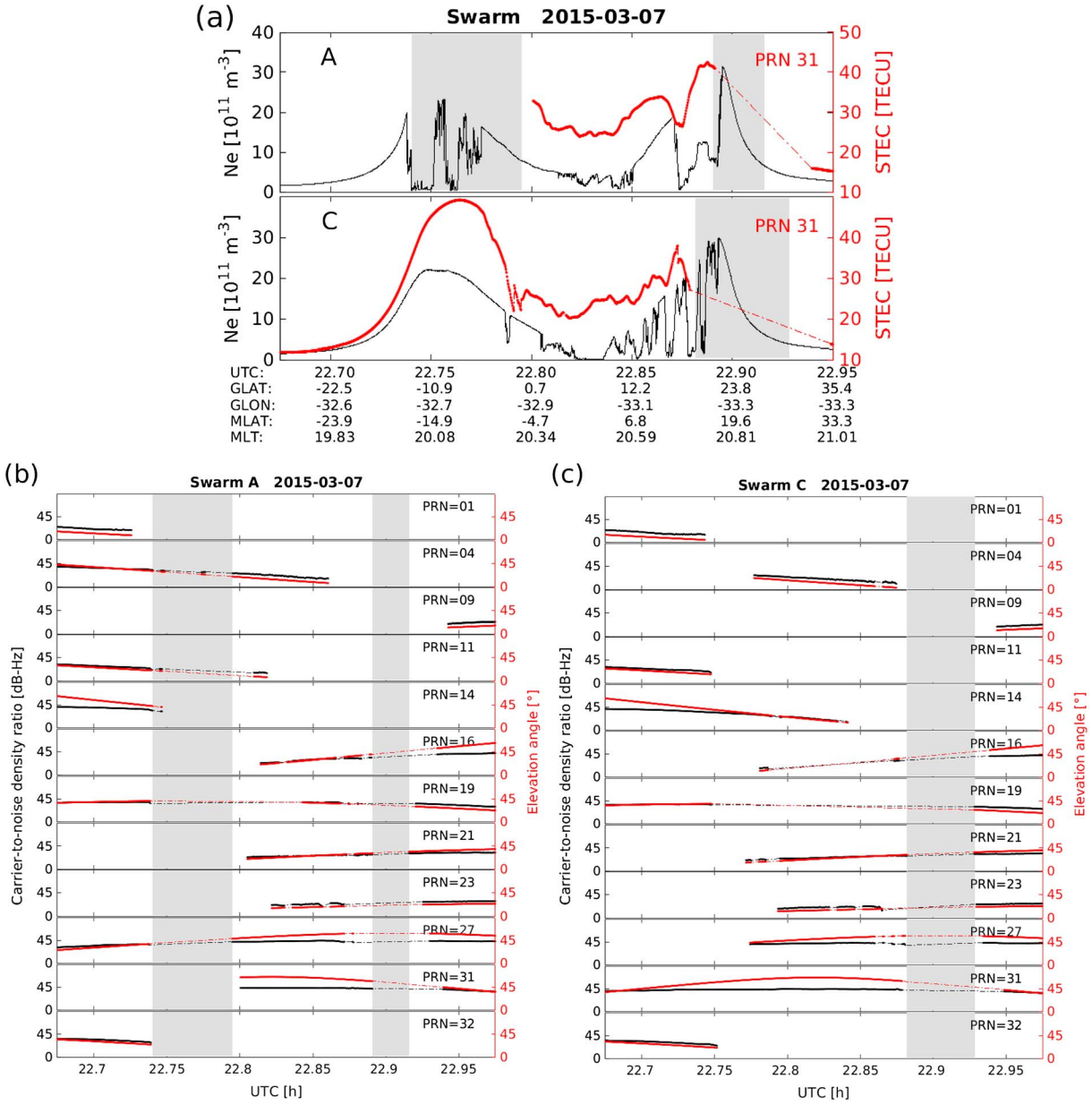

Figure 6. One example of total loss of GPS signal observed by *Swarm* A and C on 07 March 2015. (a) The in situ electron density measurements (black) and the slant TEC values from PRN = 31 (red) for the two satellites. (b) The signal strength (carrier-to-noise density ratio) and elevation angle of each visible GPS satellite observed by *Swarm* A. (c) The same as in Figure 6b but for the observation from *Swarm* C. The gray bar in each frame indicates the interval of total loss of GPS signal, and the dot-dashed intervals in Figures 6b and 6c indicate the loss of signal of the corresponding GPS satellite.

depletions between −17.6° and −10.4° MLAT (where GPS signals are totally interrupted), while the electron density variations observed by *Swarm* C are comparably smooth. The azimuth of PRN = 14 and 31 are toward the east side of *Swarm* A and C. As the strong plasma depletions are on the west side of *Swarm* C, the signals from PRN = 14 and 31 received by *Swarm* C do not pass through the region of strong plasma irregularities detected by *Swarm* A; therefore, the signal received by *Swarm* C is not affected. However, the signal from satellite PRN = 19, which is on the west side of *Swarm* A and C, was also interrupted around from 22:45 UTC onward at *Swarm* C. It indicates that its raypath from PRN = 19 received by *Swarm* C crossed the plasma irregularity region detected on board *Swarm* A. For the second interval when GPS signal total interruption is observed around 22:54 UTC, both satellites observed strong electron density variations with large depletions, and as a result GPS signals were totally interrupted for both satellites. Figure 6a also shows that the loss of

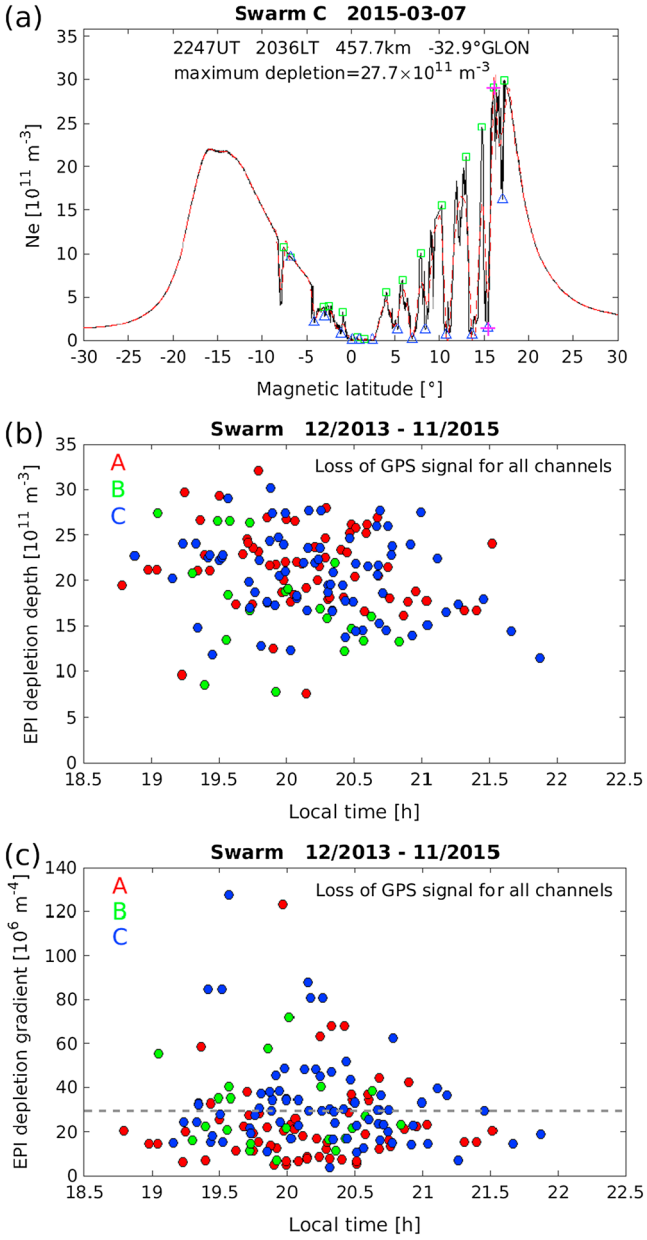

Figure 7. (a) One example of how we determine the depletion depth of equatorial plasma irregularity from the in situ measured electron density. The time and location on the top refer to the geographic equator crossing of the satellite. (b) The local time variation of the EPI depletion depth for the total loss of GPS signal events. (c) The same as in Figure 7b but for the local time distribution of the EPI depletion gradient.

GPS signal does not immediately happen when *Swarm* satellites enter the plasma irregularities, but with a certain time delay, and it also needs some time for the receiver to reacquire the GPS signal when the *Swarm* satellites leave the plasma irregularity regions. This explains why the GPS signal total interruption events are shifted a few degrees northward/southward for the ascending/descending orbital arcs, respectively, as presented in Figures 2 and 3.

3.2.2. Statistical Results

The example presented in Figure 6 indicates that the equatorial plasma irregularities, especially those with large absolute density depletions, may play an important role for causing the interruption of GPS signal. To check this, we determined the maximum density depletion of EPIs for the total loss of GPS signal events. Taking the EPI event in Figure 7a as example, we explain how to derive the maximum density depletion of EPI. The epochs, altitudes, and longitudes when the spacecraft passed the geographic equator are listed in the topside. The original 2 Hz electron density data measured by *Swarm* C is plotted with black line, and a filter has been applied to the original data series for filtering out plasma irregularities with scale lengths less than 120 km along track. From the filtered data (red-dashed line) we then find all depletion regions. The peak values between two depletion regions are then recorded from the original 2 Hz data series (marked with green squares), and then the minimum values between the two peak values are found (also from the original data series, marked with blue triangles). For each depletion region, the absolute density depletion is defined as the difference between the peak (green squares) and minimum (blue triangles) values. Finally, the maximum depletion is found from all the density depletion regions and recorded as the EPI depletion depth. In this event, the maximum density depletion was found around 15° MLAT and the EPI depletion depth (the difference between the two pink crosses) reached about $27.7 \times 10^{11}\,\mathrm{m}^{-3}$.

In this way, we derived the EPI depletion depths for all the total loss of GPS signal events, and the local time distribution of EPI depletion depths is presented in Figure 7b, marked with different colors for the three *Swarm* satellites. We see that the EPI depletion depths vary in the range from about $10 \times 10^{11}\,\mathrm{m}^{-3}$ to $30 \times 10^{11}\,\mathrm{m}^{-3}$ and slightly decrease from 19:00 to 22:00 LT. This decreasing trend of EPI depletion depths

is due to the decrease of the *F* region background electron density after sunset hours. As *Swarm* B is 50 km higher than *Swarm* A and C, the background electron density at *Swarm* B altitude is lower than that at the altitude of *Swarm* A and C. However, the effective depletion depths are about comparable between the three satellites, which imply that for causing total loss of GPS signal for a spaceborne receiver, the local absolute density depletion needs to pass a certain threshold irrespective of the level of the background electron density. It is nonetheless obvious that a significant density depletion associated with EPIs can only develop when a substantial background plasma density is reached.

The latitudinal gradient of the *F* region ionospheric electron density at the EIA crest region may also be large but with much smoother variation if there is no ionospheric plasma irregularity. This smooth varying electron density is obviously not sufficient to cause the total interruption of GPS signal for spaceborne receivers. Differently, the EPIs usually exhibit different scale sizes and the plasma density inside EPIs varies rapidly. For example, as shown in Figure 7a, the maximum density depletion of the EPI observed by *Swarm* C is about $27.7 \times 10^{11}\,m^{-3}$, and such a large-density depletion appears within a latitude range of about 0.8° (the two pink crosses appearing at 16.1° and 15.3° MLAT). If we divided the density depletion ($27.7 \times 10^{11}\,m^{-3}$) by the distance (0.8° in latitude), we derive a meridional density gradient of $36.4 \times 10^{6}\,m^{-4}$. Using this approach, we could derive the meridional depletion gradient for all the EPI events as presented in Figure 7b, and the result is presented in Figure 7c. Compared to the EPI depletion depths, the EPI depletion gradients cover a wider range, with an average value of $29.4 \times 10^{6}\,m^{-4}$ (indicated by the gray dashed line in Figure 7c), which also suggests that even with similar depletion depths, the extension of the depletion itself varies from event to event.

The importance of large-density gradients (despite the small-scale size of EPI) for causing the loss of GPS signal can also be seen from the example in Figure 6. In the southern hemisphere, *Swarm* A observed clear plasma density depletions between −17° and −10° MLAT (maximum density depletion reached $20.0 \times 10^{11}\,m^{-3}$), while the simultaneous observations from *Swarm* C are quite smooth. Considering the longitudinal separation between the two satellites (about 150 km), the density depletion with amplitude of $20.0 \times 10^{11}\,m^{-3}$ corresponds to a zonal plasma gradient of at least $13.3 \times 10^{6}\,m^{-4}$, which is of the same order as the average value of meridional plasma gradient ($29.4 \times 10^{6}\,m^{-4}$) derived above. This kind of small-scale structure of plasma irregularities with large-density gradients both in zonal and meridional directions is possibly responsible for disturbing the reception of GPS signal. When a satellite is in a deeply depleted region, steep gradients appear to exist in all directions; therefore, the loss of GPS signal then occurs for all channels, regardless of the azimuth and elevation angles of GPS satellites. Such deep electron density depletions ($>10 \times 10^{11}\,m^{-3}$) can only occur in regions of high background density. This is consistent with the report of *Whalen* [2009] that the occurrence rate of L band signal scintillation raises proportionally with the magnitude of electron density maximum of the *F* region (N_mF_2).

So far, we first identified the GPS signal total interruption events and then checked the corresponding EPI deletion depths. We will now first identify EPI events and then check for these EPI events whether a loss of GPS signal is observed. The depletion depths of all EPI events observed by *Swarm* during the considered 2 year period are presented in Figure 8a, which show a clear local time dependence, decreasing from sunset hours to postmidnight hours. This decreasing trend corresponds well to the local time variations of the *F* region background electron density (Figure 8b). Due to the prereversal enhancement of $E \times B$ drift around sunset hours, the *F* region electron density is quite large at the EIA crest region; therefore, the EPI depletion depths can reach values of about $30 \times 10^{11}\,m^{-3}$ around 20:00 LT. The upward $E \times B$ drift then gradually decreases and turns downward during later local time, causing the *F* region electron density at *Swarm* altitudes to decrease gradually. Therefore, we find EPI depletion depths mainly below $10 \times 10^{11}\,m^{-3}$ during the postmidnight hours.

In Figure 7b, showing GPS signal total interruption observed by *Swarm* satellites, the EPI depletion depths derived from the in situ electron density (except for four events) are larger than $10 \times 10^{11}\,m^{-3}$. We then took this value as a threshold (see the dashed line in Figure 8a), and found 320, 222, and 314 EPI events with depletion depths larger than this threshold during the considered 2 year period from *Swarm* A, B, and C, respectively. We further checked the GPS data and found that for 14.4%, 8.6%, and 16.6% of them a loss of GPS signal for all channels (total loss) occurred, and for 94.7%, 96.4%, and 95.9% of them a loss at least for one channel occurred, respectively, for *Swarm* A, B, and C. Coinciding with these EPIs of larger-density depletion,

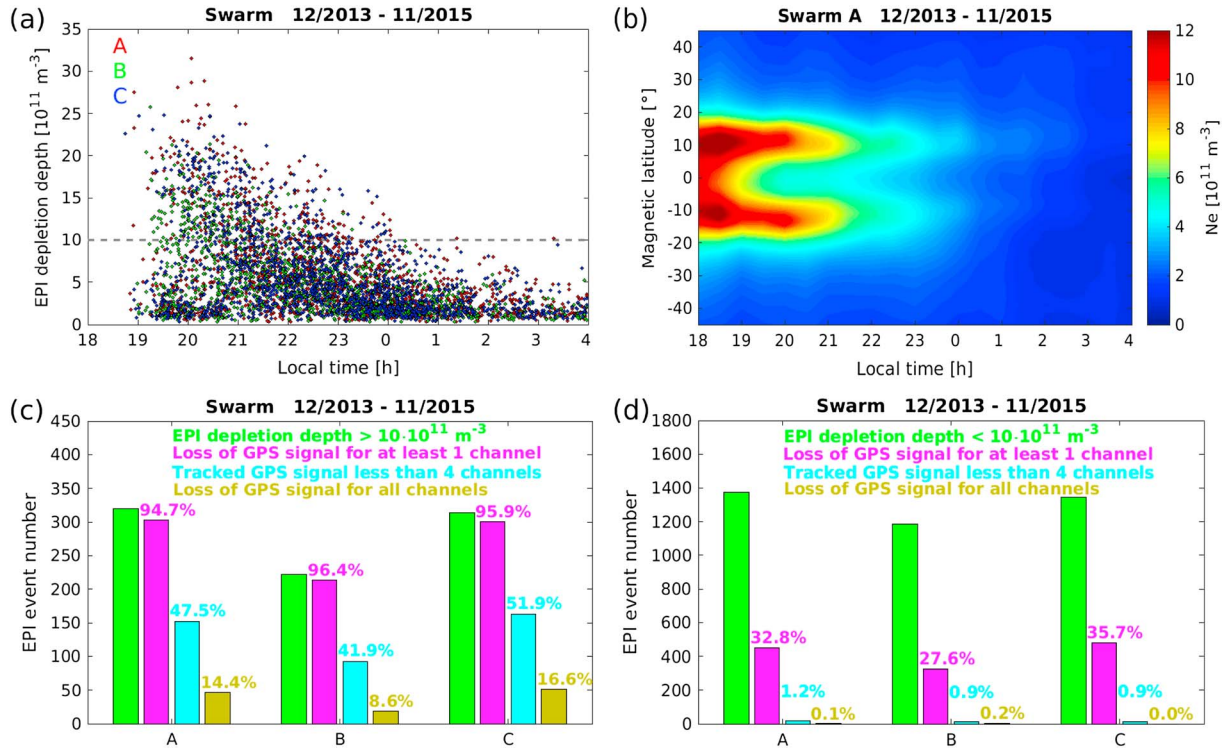

Figure 8. (a) The local time variation of the EPI depletion depth observed by *Swarm*. The different colors marked the events observed by the three satellites. (b) The magnetic latitude and local time distributions of the background electron density derived from *Swarm* A during the considered 2 year period. (c) The *Swarm*-observed EPIs with depletion depths larger than 10×10^{11} m^{-3} are indicated with green bars. The ratio of simultaneously occurring total loss of GPS signal events (at all channels), or at least for one channel, as well as the tracked GPS signal less than four channels are indicated by different colors, respectively. (d) The same as in Figure 8c but for EPI events with depletion depths less than 10×10^{11} m^{-3}.

47.5%, 41.9%, and 51.9% were found with tracked GPS satellite less than four. The result also indicates that when *Swarm* satellites encountered EPIs with depletion depths larger than 10×10^{11} m^{-3}, there is about 45% chance that the POD cannot be performed. While for those EPIs with depletion depths less than 10×10^{11} m^{-3}, only 32.8%, 27.6%, and 35.7% are observed with loss of GPS signal at least for one channel, and the chance of tracked GPS satellites less than four has reduced to only 1.2%, 0.9%, and 0.9% for the three *Swarm* satellites, respectively (Figure 8d).

Buchert et al. [2015] reported that for causing *Swarm* receiver loss of GPS signal it is not sufficient if only the relative electron density ($\Delta N_e/N_e$) is varying strongly; another crucial factor is the absolute density variation (ΔN_e needs to be large). This is consistent with our result as shown in Figures 7 and 8. The high occurrence rate of GPS signal loss when *Swarm* encountered EPIs with absolute density depletion larger than 10×10^{11} m^{-3} confirms that the ionospheric irregularities, especially those with large absolute density depletion, can directly affect the performance of the receiver on board LEO satellites. Compared to EPIs at the altitude of *Swarm* satellites (460–520 km), the EPIs at lower altitudes (closer to ionospheric F_2 peak height) exhibit probably even larger absolute density depletions. Therefore, LEO satellites flying at lower altitudes, such as CHAMP or GOCE, may even be at higher risk for loss of GPS signals. Further studies are anticipated to check the effect on other satellite mission than *Swarm*.

3.3. The Total Loss of GPS Signal at High Latitudes

During the considered 2 year period, the *Swarm* satellites observed five events with GPS signal total interruption at high latitudes. The epochs and locations of these five events are listed in Table 1. We also checked the in situ electron density measurements by *Swarm* for these high-latitude events. Figure 9 shows two examples observed by *Swarm* C on 20 April 2014 and by *Swarm* A on 06 May 2015, respectively. The gray dashed bar in each event indicates the loss of GPS signal at all channels. For both events the PLP measured in situ electron

Table 1. The Total Loss of GPS Signal Events Observed by the *Swarm* Satellites at High Latitudes

Swarm Satellites	Date	Geographic Latitude/Longitude (deg)	N_e Decrease (10^{11} m^{-3})	N_e Gradient (10^6 m^{-4})	*Kp*	*AE* (nT)
A	18/11/2014 15:03 UTC	−86.6/96.6	2.9	6.9	2.7	510
	06/05/2015 11:52 UTC	−75.0/36.5	5.9	14.1	5.3	742
B	17/03/2015 18:52 UTC	−80.5/−136.0	14.1	19.5	7.3	978
C	05/04/2014 13:16 UTC	−85.8/48.6	13.2	34.7	3.7	400
	20/04/2014 17:05 UTC	−56.4/120.7	6.9	10.7	4.0	465

density shows strong variations along track, with maximum density decreases about 7.0×10^{11} m^{-3} and 6.0×10^{11} m^{-3} (the difference between the values indicated by the two pink crosses) for the two events, respectively. When comparing the electron density measurements between *Swarm* A and C, we noticed that the latitudinal profile is quite different for each event, although the two satellites are close to each other. Similarly, the maximum density decrease and the corresponding gradient (along track) are also listed in Table 1. The average value of the maximum density depletion for these five events is about 8.6×10^{11} m^{-3}, which is indeed quite large at the ionospheric *F* region, compared to the background plasma density at high latitudes being less than at low latitudes (see also Figure 8b). The result shown here confirms that loss of GPS signal at high latitudes is also related to the large ionospheric density gradients.

Another interesting feature of the total loss of GPS signal at high latitudes events is that they are all observed in the southern hemisphere and mainly around local noon. This result is consistent with the occurrence of polar patches reported by *Noja et al.* [2013]. Based on 9 year TEC observations from the CHAMP satellite they found that the polar patches, possibly caused by local particle precipitation and the intrusion of subauroral plasma into the polar cap through tongues of ionization, were more frequently observed in the southern hemisphere, and the maximum occurrences of polar patches were found at the dayside polar cusp region. When LEO satellites, such as *Swarm*, pass through those polar patches, the GPS signal may be strongly

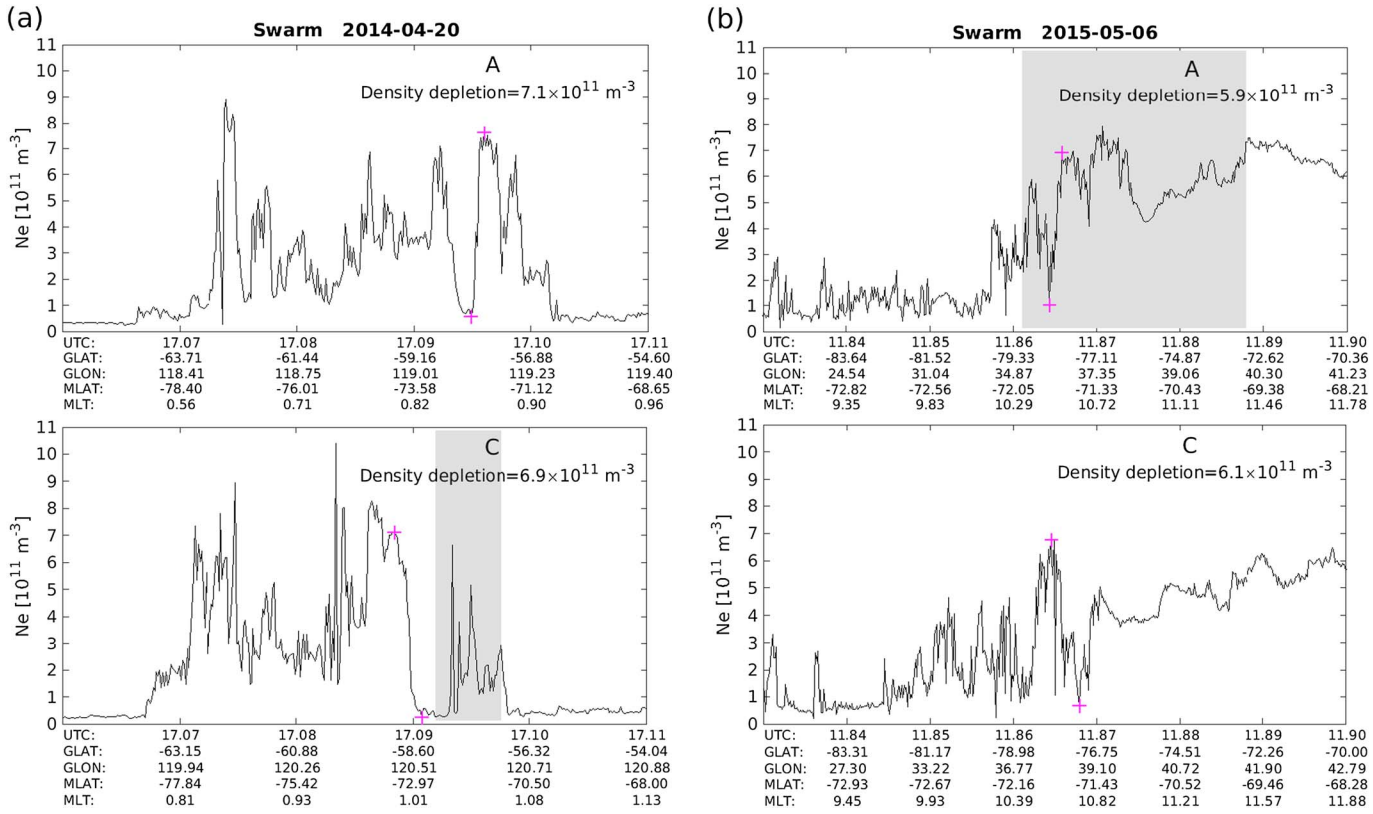

Figure 9. Examples of loss of all GPS signals (indicated by the gray bars) at high latitude observed (a) by *Swarm* C on 20 April 2014 and (b) by *Swarm* A on 06 May 2015.

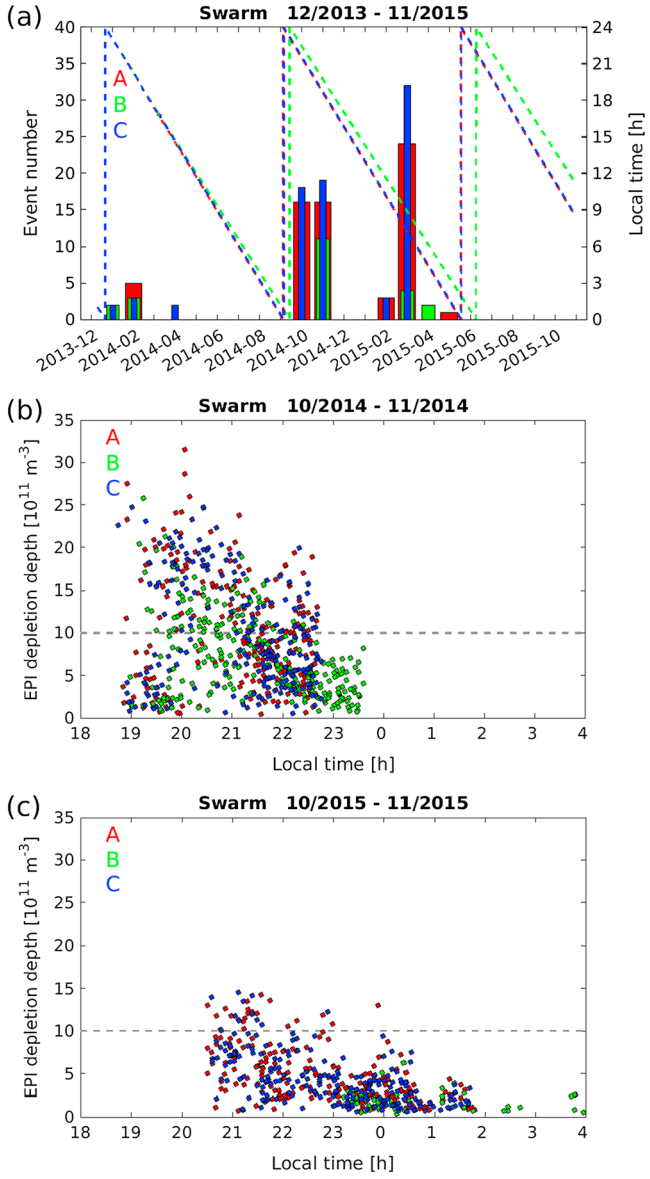

Figure 10. (a) The event number of total loss of GPS signal in each month from December 2013 to November 2015. The red, green, and blue dashed lines indicate the local time of the descending orbits at equator crossing for *Swarm* A, B, and C, respectively. (b) The local time variation of the EPI depletion depth observed by *Swarm* during October–November 2014. (c) The same as in Figure 10b but for the period of October–November 2015.

disturbed by the large plasma spatial gradients. Among the five events at high latitudes, we found the event observed by *Swarm* B, flying at higher altitudes than *Swarm* A and C, though in usually lower electron density background, happened on 17 March 2015, from 18:50:10 to 18:54:11 UTC. It is just during the so-called St. Patrick's Day storm, which is so far the largest storm of solar cycle 24, with minimum *SYM-H* reaching −234 nT [*Kamide and Kusano*, 2015]. Table 1 also provides the magnetic activity indices, *Kp* and *AE*, to characterize the global and auroral activities, respectively. For the five events the geomagnetic activities have been at moderate and disturbed levels. During storm and substorm periods enhanced energy input into the upper atmosphere, e.g., through particle precipitation, is likely to cause the ionospheric plasma density to vary strongly at high latitudes, which further affects the performance of spaceborne GPS receivers.

3.4. The Effects of Increased FOV and PLL Bandwidth on GPS Receivers

As introduced in section 2.1, the FOV and PLL bandwidth of the *Swarm* GPS receiver have been updated during the past 2 years. Figure 10a presents the number of GPS signal total interruption events in each month from December 2013 to November 2015. The red, green, and blue dashed lines indicate the local time of the descending orbits at equatorial crossing for *Swarm* A, B, and C, respectively. Taking *Swarm* C for example, the FOV was increased from 80° to 88° on 13 January 2015, but there are still a lot of events observed in March 2015. It suggests that the increased FOV does not affect the receivers' performance when *Swarm* encountered ionospheric irregularities, as the increased FOV is intended to improve the capability for receiving those GPS satellites with lower-elevation angles. When the *Swarm* satellite is inside the EPIs, the steep gradients existing in all directions will affect the signal regardless of the elevation angles of GPS ray received.

The PLL bandwidth of *Swarm* C was updated on 6 May 2015, and after that *Swarm* C observed no event with total loss of GPS signal. However, *Swarm* A and B also observed no total loss of GPS signal event after 6 May 2015, although their PLL bandwidth has been updated only later (on 8 and 10 October, respectively). Therefore, the effects of increased PLL bandwidth need to be checked with longer data set. Another possible explanation for the absence of total loss of GPS signal event after May 2015 is the reduced EPI depletion depths. Taking the months October–November as example, the descending (ascending) orbits of *Swarm* A

and C cover 19:00–23:00 (20:30–02:00) LT during the year 2014 (2015). Figures 10b and 10c show the EPI depletion depths during October–November in the 2 years observed by *Swarm*. We see clearly that the EPIs with depletion depth larger than $10\times10^{11}\,m^{-3}$ in 2014 are much more frequent and show large depletion depths (average value of $15.2\times10^{11}\,m^{-3}$) than those observed in 2015 (average value of $11.7\times10^{11}\,m^{-3}$). The decreased EPI depth relates to the ambient electron density, both caused by the reduced solar activity, as the mean solar activity index ($F_{10.7}$) during the 2 months has decreased from 152.7 solar flux unit (sfu) in 2014 to 105.2 sfu in 2015. We further checked the EPI events with depletion depth larger than $10\times10^{11}\,m^{-3}$ during October–November and found that for both years more than 95% of them *Swarm* observed loss of GPS signal at least for one channel (not shown here). However, the EPIs with smaller depletion depths observed in October–November 2015 did not cause a total loss of GPS signal at all channels for *Swarm* satellites.

4. Summary

In this study, we addressed the close relationship between ionospheric plasma irregularities and GPS signal total interruption at *Swarm* satellites. For this purpose we have investigated the first 2 year observations of the *Swarm* mission from December 2013 to November 2015. Our findings can be summarized as

1. A total loss of GPS signal at all channels is frequently observed at about 500 km. In total, *Swarm* B, flying 50 km higher than *Swarm* A and C, observed less GPS loss signal events than *Swarm* A and C. We suggest that it is due to lower background electron density, hence allowing for less deep depletions of EPIs.
2. Most of the total loss of GPS signal events are observed at low latitudes between ±5° and ±20° MLAT, at the ionization anomaly crests, forming two bands along the magnetic equator, and these events mainly appear during postsunset hours from 19:00 to 22:00 MLT. This observation is very close to that of the climatology of EPIs.
3. The total loss of GPS signal events observed by *Swarm* at low latitudes (in total 161 events) are all related to EPIs, which almost all (except for four events) show absolute density depletions larger than $10\times10^{11}\,m^{-3}$. Coinciding with EPIs of density depletions larger than $10\times10^{11}\,m^{-3}$ within a 2 year period, the *Swarm* satellites observed up to 95% loss of GPS signal at least for one channel and 45% of tracked GPS signals less than four (when POD cannot be performed). While for those EPIs with density depletions less than $10\times10^{11}\,m^{-3}$, the chance of tracked GPS signals less than four has reduced to only 1.0%. Our result confirms that the EPI with large absolute density depletion plays a crucial role for causing loss of GPS signal for LEO satellites.
4. Some total loss of GPS signal has also been observed at high latitude, mainly around local noon. And these events are possibly related to the large spatial density gradient at high latitudes, e.g., due to polar patches or increased geomagnetic/auroral disturbances.

Acknowledgments
We want to thank Ji-Sheng Xu, Xingxing Li, Guram Kervashvili, and Jaeheung Park for their fruitful discussions on GPS and ionospheric conditions. We thank Christian Siemes for his advice on the *Swarm* GPS receiver performance. The European Space Agency is acknowledged for providing the *Swarm* data. The official *Swarm* website is http://earth.esa.int/Swarm, and the server for *Swarm* data distribution is ftp://Swarm-diss.eo.esa.int. This work is supported by DFG priority program 1788 "Dynamic Earth."

References

Aarons, J. (1982), Global morphology of ionospheric scintillations, *Proc. IEEE*, *70*, 360–378.
Aarons, J., and S. Basu (1994), Ionospheric amplitude and phase fluctuations at the GPS frequencies, paper presented at ION GPS, Inst. of Navig., Salt Lake City, Utah.
Basu, S., S. Basu, J. P. Mullen, and A. Bushby (1980), Long-term 1.5 GHz amplitude scintillation measurements at the magnetic equator, *Geophys. Res. Lett.*, *7*, 259–262, doi:10.1029/GL007i004p00259.
Basu, S., K. M. Groves, S. Basu, and P. J. Sultan (2002), Specification and forecasting of scintillations in communication/navigation links: Current status and future plans, *J. Atmos. Sol. Terr. Phys.*, *64*, 1745–1754.
Brahmanandam, P. S., G. Uma, J. Y. Liu, Y. H. Chu, N. S. M. P. Latha Devi, and Y. Kakinami (2012), Global S_4 index variations observed using FORMOSAT-3/COSMIC GPS RO technique during a solar minimum year, *J. Geophys. Res.*, *117*, A09322, doi:10.1029/2012JA017966.
Buchert, S., F. Zangerl, M. Sust, M. André, A. Eriksson, J. Wahlund, and H. Opgenoorth (2015), *SWARM* observations of equatorial electron densities and topside GPS track losses, *Geophys. Res. Lett.*, *42*, 2088–2092, doi:10.1002/2015GL063121.
Burke, W. J., L. C. Gentile, C. Y. Huang, C. E. Valladares, and S. Y. Su (2004), Longitudinal variability of equatorial plasma bubbles observed by DMSP and ROCSAT-1, *J. Geophys. Res.*, *109*, A12301, doi:10.1029/2004JA010583.
Carter, B. . A., K. Zhang, R. Norman, V. . V. Kumar, and S. Kumar (2013), On the occurrence of equatorial *F*-region irregularities during solar minimum using radio occultation measurements, *J. Geophys. Res. Space Physics*, *118*, 892–904, doi:10.1002/jgra.50089.
Dymond, K. . F. (2012), Global observations of L band scintillation at solar minimum made by COSMIC, *Radio Sci.*, *47*, RS0L18, doi:10.1029/2011RS004931.
Emmert, J. T., A. D. Richmond, and D. P. Drob (2010), A computationally compact representation of magnetic-apex and quasi-dipole coordinates with smooth base vectors, *J. Geophys. Res.*, *115*, A08322, doi:10.1029/2010JA015326.
Huang, C. Y., W. J. Burke, J. S. Machuzak, L. C. Gentile, and P. J. Sultan (2001), DMSP observations of equatorial plasma bubbles in the topside ionosphere near solar maximum, *J. Geophys. Res.*, *106*(A5), 8131–8142, doi:10.1029/2000JA000319.

Huang, C.-S., O. de La Beaujardiere, P. A. Roddy, D. E. Hunton, J. Y. Liu, and S. P. Chen (2014), Occurrence probability and amplitude of equatorial ionospheric irregularities associated with plasma bubbles during low and moderate solar activities (2008–2012), *J. Geophys. Res. Space Physics*, *119*, 1186–1199, doi:10.1002/2013JA019212.

Jakowski, N., Y. Beniguel, G. De Franceschi, M. H. Pajares, K. S. Jacobsen, I. Stanislawska, L. Tomasik, R. Warnant, and G. Wautelet (2012), Monitoring, tracking, and forecasting ionospheric perturbations using GNSS techniques, *J. Space Weather Space Clim.*, *2*, A22, doi:10.1051/swsc/2012022.

Kamide, Y., and K. Kusano (2015), No Major Solar Flares but the Largest Geomagnetic Storm in the Present Solar Cycle, *Space Weather*, *13*, 365–367, doi:10.1002/2015SW001213.

Kelley, M. C. (2009), *The Earth's Ionosphere: Electrodynamics and Plasma Physics*, 2nd ed., Elsevier, New York.

Kil, H., and R. A. Heelis (1998), Global distribution of density irregularities in the equatorial ionosphere, *J. Geophys. Res.*, *103*(A1), 407–417, doi:10.1029/97JA02698.

Kintner, P. M., B. M. Ledvina, E. R. de Paula, and I. J. Kantor (2004), Size, shape, orientation, speed, and duration of GPS equatorial anomaly scintillations, *Radio Sci.*, *39*, RS2012, doi:10.1029/2003RS002878.

Kintner, P. M., B. M. Ledvina, and E. R. de Paula (2007), GPS and ionospheric scintillations, *Space Weather*, *5*, S09003, doi:10.1029/2006SW000260.

Noja, M., C. Stolle, J. Park, and H. Lühr (2013), Long-term analysis of ionospheric polar patches based on CHAMP TEC data, *Radio Sci.*, *48*, 289–301, doi:10.1002/rds.20033.

Park, J., M. Noja, C. Stolle, and H. Lühr (2013), The Ionospheric Bubble Index deduced from magnetic field and plasma observations onboard *Swarm*, *Earth Planets Space*, *65*(11), 1333–1344, doi:10.5047/eps.2013.08.005.

Pradipta, R., C. E. Valladares, B. A. Carter, and P. H. Doherty (2016), Interhemispheric propagation and interactions of auroral traveling ionospheric disturbances near the equator, *J. Geophys. Res. Space Physics*, *121*, 2462–2474, doi:10.1002/2015JA022043.

Richmond, A. D. (1995), Ionospheric electrodynamics using magnetic apex coordinates, *J. Geomagn. Geoelectr.*, *47*, 191–212.

SBAS Ionospheric Working Group (2010), Effect of ionospheric scintillations on GNSS—A white paper. [Available at http://waas.stanford.edu/papers/IWG/sbas_iono_scintillations_white_paper.pdf.]

Stolle, C., H. Lühr, M. Rother, and G. Balasis (2006), Magnetic signatures of equatorial spread *F* as observed by the CHAMP satellite, *J. Geophys. Res.*, *111*, A02304, doi:10.1029/2005JA011184.

Stolle, C., H. Lühr, and B. G. Fejer (2008), Relation between the occurrence rate of ESF and the equatorial vertical plasma drift velocity at sunset derived from global observations, *Ann. Geophys.*, *26*(12), 3979–3988.

Su, S.-Y., C. H. Liu, H. H. Ho, and C. K. Chao (2006), Distribution characteristics of topside ionospheric density irregularities: Equatorial versus midlatitude regions, *J. Geophys. Res.*, *111*, A06305, doi:10.1029/2005JA011330.

Sust, M., F. Zangerl, O. Montenbruck, S. Buchert, and A. G. Rodriguez (2014), Spaceborne GNSS-receiving system performance prediction and validation, In: NAVITEC 2014, ESA Workshop on Satellite Navigation Technologies and GNSS Signals and Signal Processing, 3-5 Dec 2014, Noordwijk, The Netherlands.

van den IJssel, J., J. Encarnação, E. Doornbos, and P. Visser (2015), Precise science orbits for the *Swarm* satellite constellation, *Adv. Space Res.*, *56*(6), 1042–1055, doi:10.1016/j.asr.2015.06.002.

van den Ijssel, J., B. Forte, and O. Montenbruck (2016), Impact of *Swarm* GPS receiver updates on POD performance, *Earth Planets Space*, 68–85, doi:10.1186/s40623-016-0459-4.

Whalen, J. A. (2009), The linear dependence of GHz scintillation on electron density observed in the equatorial anomaly, *Ann. Geophys.*, *27*, 1755–1761, doi:10.5194/angeo-27-1755-2009.

Whitney, H. E., and S. Basu (1977), The effect of ionospheric scintillation on VHF/UHF satellite communications, *Radio Sci.*, *12*(1), 123–133, doi:10.1029/RS012i001p00123.

Xiong, C., J. Park, H. Lühr, C. Stolle, and S. Y. Ma (2010), Comparing plasma bubble occurrence rates at CHAMP and GRACE altitudes during high and low solar activity, *Ann. Geophys.*, *28*, 1647–1658, doi:10.5194/angeo-28-1647-2010.

Xiong, C., C. Stolle, H. Lühr, J. Park, B. G. Fejer, and G. N. Kervalishvili (2016), Scale analysis of the equatorial plasma irregularities derived from *Swarm* constellation, *Earth Planets Space*, doi:10.1186/s40623-016-0502-5.

Yue, X., W. S. Schreiner, N. M. Pedatella, and Y.-H. Kuo (2016), Characterizing GPS radio occultation loss of lock due to ionospheric weather, *Space Weather*, *14*, 285–299, doi:10.1002/2015SW001340.